Effective Production of Fluorescent Nanodiamonds Containing Negatively-Charged Nitrogen-Vacancy Centers by Ion Irradiation

Shingo Sotoma,[a]
Yohsuke Yoshinari,[b]
Ryuji Igarashi,[a]
Akiyoshi Yamazaki,[c,1]
Shige H. Yoshimura,[d]
Hidehito Tochio,[a]
Masahiro Shirakawa[a,b]
Yoshie Harada[b,*]

[a]Department of Molecular Engineering, Graduate School of Engineering, Kyoto University, Nishikyo-ku, Kyoto 615-8510, Japan
[b]Institute for Integrated Cell-Material Sciences (WPI-iCeMS), Kyoto University, Yoshida-Honmachi, Sakyo-ku, Kyoto 606-8501, Japan
[c]Takasaki Advanced Radiation Research Institute, Japan Atomic Energy Agency, 1233 Watanuki-machi, Takasaki, Gunma 370-1292, Japan
[d]Graduate School of Biostudies, Kyoto University, Yoshida-konoe-cho, Sakyo-ku, Kyoto 606-8501, Japan

*Corresponding author:
Institute for Integrated Cell-Material Sciences (WPI-iCeMS), Kyoto University, Yoshida-Honmachi, Sakyo-ku, Kyoto 606-8501, Japan, Tel: +81-75-753-9841,
Email: harada.yoshie.4r@kyoto-u.ac.jp

[1]Present address:
Tandem Accelerator Complex, Research Facility Center for Science and Technology, University of Tsukuba, 1-1-1 Tennodai, Tsukuba, Ibaraki 305-8577, Japan

Author Contributions:
S.S. and Y.Y. contributed equally.

Keywords:
Nanodiamond
Negatively-charged nitrogen-vacancy center

Optically detected magnetic resonance
Ion irradiation
Raman spectroscopy

Abstract

Fluorescence from negatively-charged nitrogen-vacancy centers (NV^-s) in diamonds has unique optical properties with none of the undesirable effects such as photo-bleaching and photo-blinking. In addition, the spin-dependent fluorescence intensity of NV^- allows us to perform optically detected magnetic resonance (ODMR) investigation for evaluating the presence of NV^-s and for the electronic local environment. In this work, we irradiated H^+, He^+, Li^+ and N^+ ions to nanodiamonds with a median size of 26 nm at various irradiation energies and doses for improving the NV^-s concentration. ODMR observations of the nanodiamonds showed that ion irradiation increased the number of nanodiamonds containing NV^-s up to 200 ppm, whereas without ion irradiation, only few NV^-s were found. The number of nanodiamonds containing NV^-s at various ion irradiation doses was not monotonous, but had maxima at certain irradiation doses. These results suggest a competition in two opponent roles of vacancies, effective for pairing with nitrogen atoms and as defects for developing damage in crystalline. We also found that sharp and strong ODMR signals were obtained from nanodiamonds irradiated at the optimal condition for the highest yield of NV^-s. We concluded that He^+ ion irradiations with 60 or 80 keV at a dose of 1×10^{13} ions per cm^2 are the conditions required for the most efficient production of a high quantity of nanodiamonds containing NV^-s.

1. Introduction

Fluorescent nanodiamonds (FNDs) have been attracting much attention as new bio-imaging probes due to their unique optical properties. The negatively-charged nitrogen-vacancy color center (NV^-) in FNDs, which is formed by a substitutional nitrogen atom combining with an adjacent vacancy, is responsible for fluorescence that is emitted in the near-infrared region (600-800 nm) with a high quantum yield of ~0.7.[1,2] Its well-known photo-stability of displaying neither photo-blinking nor photo-bleaching enables long-term *in vivo* and *in vitro* imaging, which is not readily achieved by commonly used fluorescent agents such as organic dyes and fluorescent proteins.[3–5] It has also been reported that FNDs are highly bio-compatible and non-toxic to various kinds of cell types,

and are thus superior to quantum dots which often show cyto-toxicity.[6,7] These advantages of FNDs over conventional fluorescent dyes could make them a potential candidate for optical bio-imaging probes.[5,8,9]

Optically detected magnetic resonance (ODMR) has been demonstrated for detection of a single NV^- at ambient conditions[10], and significant attention has been paid in the field of quantum information[11], magnetic sensing[12,13] and bio-application.[14,15] In particular, advanced applications in the nano-scale sensing of magnetic[16,17] and electric fields[18] and temperature[19] require a long-time coherence of spin state, which strongly depends on the quality of the diamond matrix. For this reason, methods for synthesizing high quality nanodiamonds and the efficient production of NV^-s are highly desired. Here, we report the effects of ion irradiation on the production of NV^-s in nanodiamonds.

There are two types of nitrogen-vacancy centers (NVCs), each with a different charged state.[20,21] One is a neutral NVC (NV^0, electron spin: S = 1/2), while the other is a negatively-charged NVC (NV^-, electron spin: S = 1), represented by zero-phonon lines at 575 nm and 637 nm respectively.[22,23] Both NVCs emit fluorescence, but only the NV^- allows for measurement by ODMR. The ground state of NV^- is a spin-triplet, and the spin sublevels, $m_s = 0$ and $m_s = \pm 1$ are split by 2.87 GHz. The spin sublevels $m_s = \pm 1$ are degenerated in the absence of an external magnetic field. Microwave (MW) irradiation at this frequency induces electron spin magnetic resonance between $m_s = 0$ and degenerated $m_s = \pm 1$ spin levels, which results in a reduction of the fluorescence intensity from NV^- due to spin-dependent intersystem crossing.[10] On the other hand, NV^0 is insensitive to MW irradiation. By comparing the fluorescence intensity upon MW irradiation, we can distinguish the two types of NVCs, as shown later.

In general, the concentration of NVCs in diamond is on the order of sub ppm.[16] The existence probability of NVCs contained in nanodiamonds is lower than that in bulk diamonds, because vacancies are annihilated at the surface.[24] In order to increase the concentration of NVCs in nanodiamonds, the method of ion irradiation is commonly used for creating carbon vacancies.[3,25] In this technique, ionized atoms are accelerated and are allowed to penetrate into nanodiamonds, where collisions of the ions with atoms force the carbon atoms to be expelled, resulting in the creation of vacancies. Subsequent thermal annealing at 800 ^oC leads to trapping of moving vacancies by nitrogen atoms which pre-exist in the diamond lattice, thereby forming an NVC.[26] Although this method is quite effective, optimal conditions for producing a high quantity of NV^-s in nanodiamonds are still unknown. In this study, we also investigated how ion irradiation affects the production of nanodiamonds containing NV^-s, and their ODMR spectra when

irradiated by H^+, He^+, Li^+ and N^+ ions. Furthermore, we elucidated the optimal irradiation condition.

2. Experimental Section

2.1 Sample preparation

In our experiments, we used synthetic type Ib nanodiamonds which contain typically 100 ppm nitrogen atoms (Micron+ MDA Element Six). A suspension of nanodiamonds in Milli-Q water was centrifuged at 15,000 rpm for 20 min, and the supernatant was freeze-dried. The median size of the nanodiamond particles was determined by dynamic light scattering (DLS) to be 25.9 nm (Fig. 1). 2 µl of a nanodiamond suspension in Milli-Q water at a concentration of 2 mg/ml was dropped on the surface of a silicon wafer measuring1 cm^2, and subsequently spin-coated at 7000 rpm for 20 s. To estimate the number of nanodiamonds on the silicon wafer, we carried out atomic force microscope (AFM) measurements and obtained the images of prepared samples (Fig. S1), from which we directly counted the number of nanodiamonds which cover an area of 1 mm^2 on a wafer to be 1.6×10^6 particles.

2.2 Ion irradiation

The samples were irradiated by H^+, He^+, Li^+ and N^+ ions in vacuum at ~ 10^{-5} Pa under various energy and dose conditions at Takasaki Advanced Radiation Research Institute JAEA. The ion penetration depth and the number of vacancies created per incident ion at a given irradiation energy were evaluated in advance by SRIM (http://www.srim.org/) (Table 1). For obtaining desired dosages, ion beam currents in the range of ~0.1 nA to ~300 nA and the exposure times were adjusted. Under the conditions employed in this experiment, most ions passed through the nanodiamond arrays. After the irradiation, the samples were thermally annealed at 800 °C under a reduced pressure of ~ 1 Pa for2 h, for the purpose of pairing nitrogen atoms and vacancies. Since the graphite layer on the surfaces of nanodiamonds interferes with fluorescence emission from NV^-s, the layer was removed by oxidizing at 500 °C under atmospheric conditions for 2 h.

2.3 Count of Nanodiamonds containing NV^-s and measurement of its ODMR spectra

The number of nanodiamonds containing NV^-s generated by ion irradiation was counted by the following method using a home-built fluorescence microscope. In our experimental set-up, the field of view was illuminated with a 532-nm Nd:YAG laser at 7 mW, and fluorescence images (40 µm × 40 µm) were measured by an electron multiplying charge coupled device (EMCCD) camera. The emitted light was collected by an oil immersion 60× objective lens (NA=1.49) and passed through a dichroic mirror centered at 575 nm and a long (short)-wave pass filter longer than 590 nm (shorter than 842 nm)

to detect the intrinsic signal. The microscope was equipped with a computer-controlled moving stage. Firstly, the sample was roughly scanned in a broad range of areas in steps of 50 μm. At each position, fluorescence images were measured while MW was swept point-by-point across the resonant frequency from 2.865 to 2.875 GHz. The intrinsic fluorescence from NV^-s was deduced by the selective imaging protocol reported by Igarashi et al..[15] This procedure provides a conventional fluorescence image as well as a selective one, the latter displaying only a signal arising from NV^- fluorescence. Typical obtained images are shown in Fig. 2. After the pre-scanning, the allocation numbers of images which contained the fluorescence from NV^-s were listed and stored. In order to precisely measure the entire ODMR spectrum for each nanodiamond containing NV^-s in the allocated field, a second run was performed with the MW swept widely from 2.820 to 2.920 GHz point-by-point. After acquiring hundreds of images in the latter process, the number of nanodiamonds containing NV^-s was counted. The extraction of intrinsic signals was done by setting a threshold for the signal intensity, so as to pick up the nanodiamonds which contain roughly more than two NV^-s. Below, we abbreviate a particular condition of ion irradiation by the notation [ion species, energy, dose per cm^2], such as [He^+, 20 keV, 1×10^{13}].

3. Results and Discussion

The numbers of nanodiamonds containing NV^-s produced per mm^2 as a function of energy and ion dose for H^+, He^+, Li^+ and N^+ irradiation are listed in Table 2. Fig. 3 shows a bar chart representation of the values given in Table 2. The results of H^+ irradiation show no or very few instances of nanodiamonds containing NV^-s after irradiation with less than or equal to 1×10^{12} ions per cm^2. Production of nanodiamonds containing NV^-s increased as ion dose increased, but doses higher than 1×10^{14} ions per cm^2 caused a decline in NV^- production. This turning point indicates the optimal condition for NV^- production by H^+ ion irradiation. The results for He^+ ion irradiation were found to be similar to those observed for H^+ irradiation, with the dose being one order lower in magnitude. Li^+ ion irradiation showed a significantly lower efficiency of NV^- production, and N^+ ion irradiation was observed to produce no NV^-s (not shown). The results indicate that the ion doses exert significant influence on NV^- production, and that the optimal conditions appear to be shifted to lower doses as the irradiation energy decreases. Considering our irradiation energies and the corresponding depth profiles (Table 1), some of the incident ions may be trapped in the nanodiamonds at a finite probability and contribute effectively to create vacancies. As a consequence, we found that the optimal conditions for producing nanodiamonds containing NV^-s are 1×10^{14} ions per cm^2 for H^+

and 1×10^{13} ions per cm^2 for He^+.

The number of nanodiamonds containing NV^-s produced by ion irradiation was estimated as follows. In our experimental set-up, approximately 1.6×10^6 nanodiamond particles cover an area of 1 mm^2 on a silicon wafer. As 322 nanodiamonds containing NV^-s were observed for [H^+, 20 keV, 1×10^{14}], one nanodiamond containing NV^-s is created per 5×10^3 particles, yielding a density of 200 ppm. This number is a marked improvement as compared to the case of non-irradiated nanodiamonds, in which no NV^-s were observed.

In order to investigate the damage in the diamond crystal due to ion irradiations, the ODMR spectra of the nanodiamonds containing NV^-s were evaluated, since the line shape of the magnetic resonance spectra is sensitive to distortions in the crystal lattice around NV^-s. We analyzed the spectra taken for NV^-s created by H^+, He^+ and Li^+ irradiation at various conditions. Each ODMR spectrum was then fitted to a Gaussian function (Figure 4a):

$$f(\nu) = const - \alpha \exp\{-\frac{1}{2}(\frac{\nu-\nu_0}{\Delta\nu})^2\} \ , \quad (1)$$

where ν, ν_0, α and $\Delta\nu$ are the MW frequency, resonance frequency, depth and frequency width, respectively. We focused on the depth α and width $\Delta\nu$ because they are good indicators for the evaluation of inhomogeneity around NV^-s. In particular, electrical inhomogeneity caused by ion irradiation induces a distribution of the local crystal field around NV^-s, thus causing broad line width and weak signal depth in the spectrum. As shown in Fig. 4b and 4c, the histograms of the parameters α and $\Delta\nu$ of the spectra of ion irradiated nanodiamonds have maxima around 3% and 12 MHz, and spread asymmetrically from 1% to 10% and from 5 MHz to 30 MHz, respectively. We further made in Fig. 4d a correlation plot between these two parameters to investigate the effects of ion irradiation on the ODMR spectra, and divided the domain into six segments (classes 1 to 6). This classification made it easy to compare the spectral profiles belonging to these categories. For example, the spectra of samples at [He^+, 80 keV, 1×10^{13}] (blue dots in Fig. 4d) shown mainly in the lower-right area (classes 5 or 6) exhibit strong signal depth and narrow widths. These features indicate that the irradiation condition produces NV^-s without large perturbation of the crystalline lattice. In contrast, the spectra of samples at [He^+, 80 keV, 1×10^{14}] (green dots in Fig. 4d) shown in the upper-left area (classes 1 or 3) show shallow and broad signals. Fig. 4e displays examples of ODMR spectra picked from each class for comparison. The spectra from class 5 (brown) or 6 (orange) show strong and narrow signals, which are suitable for application using ODMR. In contrast, those from class 1 (blue) yielded shallow and broad signals, thus indicating that such NV^- is not suitable. Consequently, a search for optimal conditions

for irradiation was conducted by calculating the ratio of the number of NV^-s classified in class 5 or 6 to the total number of NV^-s. The results are listed in Table 3. The most suitable condition for generating nanodiamonds giving high-quality ODMR was found to be [He^+, 60 or 80 keV, 1×10^{13}], where more than 40% of the generated NV^-s belonged to class 5 or 6. [H^+, 40, 60 or 80 keV, 1×10^{14}] and [He^+, 40 keV, 1×10^{13}] are in second place, with approximately 30% of the generated NV^-s located in class 5 or 6. These conditions coincide with those producing the largest number of NV^-s, as seen in Fig. 3. Li^+ irradiation was not effective both for producing a large number of NV^-s and for the creation of NV^-s yielding high quality ODMR signals.

We also carried out Raman spectroscopic measurements to elucidate why the irradiation with heavy ion species or an excess dose of lighter ions leads to a decrease in the generation of NV^-s and the low quality of ODMR. Raman spectroscopy enables us to evaluate the crystalline quality of diamonds.[27,28] Diamond has a strong and sharp Raman signal at 1332 cm^{-1} attributed to sp^3 bonding carbon, while disorders of the crystal lattice cause the appearance of a broad signal at ~1500 cm^{-1}.

Fig. 5 shows examples of Raman spectra of the nanodiamonds containing NV^-s created in this study. At all irradiation energies, the 1332 cm^{-1} sp^3 peak decreased with an increase in ion irradiation dose, while the band around 1450 cm^{-1}, which is attributed to disorders of crystal lattices, increased. We evaluated the quality of the crystal structure of the nanodiamonds containing NV^-s in terms of the intensity of the sp^3 diamond peak divided by that of the disorder-originating band peak (Table 4). The ratio decreased as the irradiation dose increased, indicating that the high dose perturbed the crystal structures. These results suggest that the generation of vacancies and the disruption of the crystalline structure are competitive events. Generation of vacancies contributes to the formation of NV^-s until ion irradiation reaches the optimal dose, after which disruption of the crystal structure is dominant, preventing the formation of NV^-s and enhancing the electrical inhomogeneity that causes weak and broad ODMR signals. For similar reasons, ion irradiation of heavy ion species not only creates excess vacancies in nanodiamonds, but also significantly disrupts the crystalline structure, resulting in no functional NV^-s.

Conclusion

We explored the optimal conditions of ion irradiation for creating nanodiamonds containing NV^-s with a median particle size of 26 nm. The obtained best conditions were He^+ ion irradiation at 60 keV or 80 keV with a dose of 1×10^{13} ions per cm^2 for the production of high-quantity and high-quality nanodiamonds containing NV^-s. The

consequent NV^-s exhibited strong intensities and narrow widths in ODMR spectra, which is generally an indication of good crystalline. We also demonstrated that irradiation with heavy ion species or an excessive ion dose leads to the destruction of nanodiamond crystals, resulting in a decrease in the quantity and quality of NV^-s. In particular, Raman spectroscopy clearly revealed the gradual deterioration of crystalline upon those irradiations, evidenced by the observation of the intensity shifted gradually from the diamond sp^3 peak to the band characteristic of crystal disorder. The optimal irradiation condition seems to imply a subtle competition of the role of vacancies not only effective for pairing with nitrogen atoms but also as defects for developing damage in crystalline. Our experimental data supplies a guideline for optimal conditions of ion irradiation and facilitates a wide range of studies involving NV^-s.

Supplementary data to this article can be found online at http://dx.doi.org/10.1016/j.diamond.2014.07.011.

Acknowledgement

This research was supported by the World Premier International Research Center Initiative (WPI), MEXT Japan, Core Research for Evolutional Science and Technology, Japan Science and Technology Agency. Open Advanced Research Facilities Initiative of Japan Atomic Energy Agency, Japan Society for the Promotion of Science under Funding Program for Next-Generation World Researchers (NEXT Program), and Grant-in-Aid for Scientific Research on Innovative Areas.

Prime novelty statement

In this paper, we propose an efficient production method for nanodiamonds containing NV^-s by means of an ion irradiation technique. ODMR for NV^- has attracted a lot of attention for its variety of applications, however, appropriate irradiation condition for creating NV^-s still remains unknown. This is the first work reporting the ion irradiation conditions for producing high-quantity and high-quantity nanodiamonds containing NV^-s.

Graphical abstract

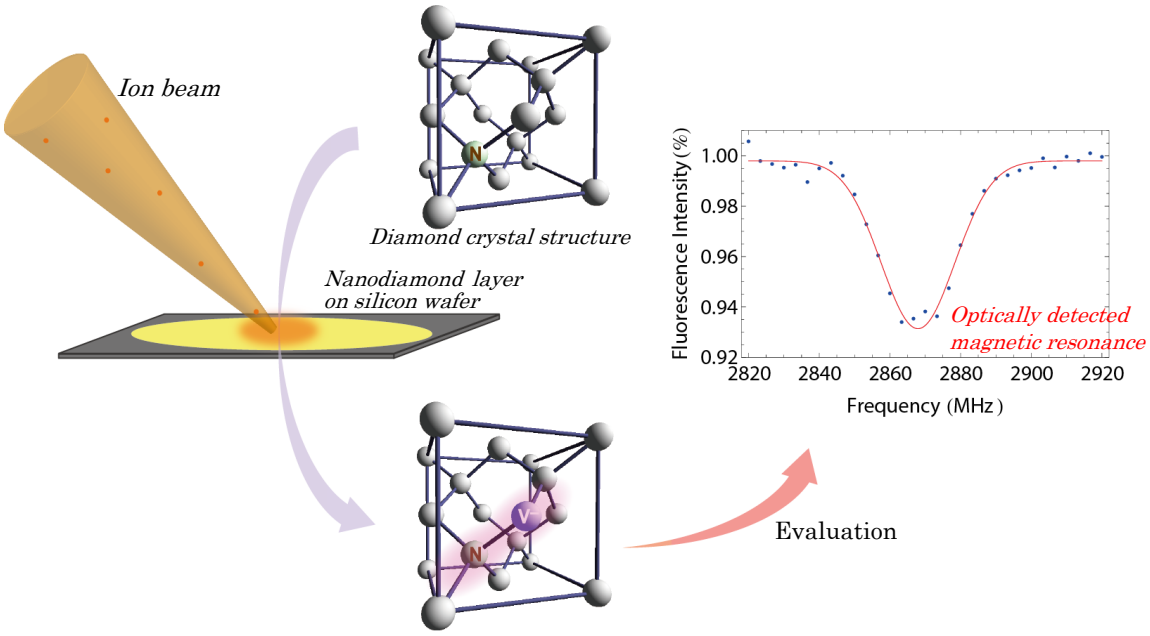

Legend to graphical abstract:

Schematic diagram of ion irradiation for producing NV^-s and evaluation by optically detected magnetic resonance (ODMR).

References

[1] S.-J. Yu, M.-W. Kang, H.-C. Chang, K.-M. Chen, Y.-C. Yu, Bright fluorescent nanodiamonds: no photobleaching and low cytotoxicity., J. Am. Chem. Soc. 127 (2005) 17604–5.

[2] T. Gaebel, I. Popa, a Gruber, M. Domhan, F. Jelezko, J. Wrachtrup, Stable single-photon source in the near infrared, New J. Phys. 6 (2004) 98–98.

[3] Y.-R. Chang, H.-Y. Lee, K. Chen, C.-C. Chang, D.-S. Tsai, C.-C. Fu, et al., Mass production and dynamic imaging of fluorescent nanodiamonds., Nat. Nanotechnol. 3 (2008) 284–8.

[4] C.-C. Fu, H.-Y. Lee, K. Chen, T.-S. Lim, H.-Y. Wu, P.-K. Lin, et al., Characterization and application of single fluorescent nanodiamonds as cellular biomarkers., Proc. Natl. Acad. Sci. U. S. A. 104 (2007) 727–32.

[5] J.-I. Chao, E. Perevedentseva, P.-H. Chung, K.-K. Liu, C.-Y. Cheng, C.-C. Chang, et al., Nanometer-sized diamond particle as a probe for biolabeling., Biophys. J. 93 (2007) 2199–208.

[6] A.M. Schrand, H. Huang, C. Carlson, J.J. Schlager, E. Omacr Sawa, S.M. Hussain, et al., Are diamond nanoparticles cytotoxic?, J. Phys. Chem. B. 111 (2007) 2–7.

[7] H. Huang, E. Pierstorff, E. Osawa, D. Ho, Active nanodiamond hydrogels for chemotherapeutic delivery., Nano Lett. 7 (2007) 3305–14.

[8] P. Sharma, S. Brown, G. Walter, S. Santra, B. Moudgil, Nanoparticles for bioimaging., Adv. Colloid Interface Sci. 123-126 (2006) 471–85.

[9] Y.-C. Lin, E. Perevedentseva, L.-W. Tsai, K.-T. Wu, C.-L. Cheng, Nanodiamond for intracellular imaging in the microorganisms in vivo., J. Biophotonics. 5 (2012) 838–47.

[10] C. von B. A. Gruber, A. Dräbenstedt, C. Tietz, L. Fleury, J. Wrachtrup, Scanning Confocal Optical Microscopy and Magnetic Resonance on Single Defect Centers, Science (80-.). 276 (1997) 2012–2014.

[11] H. Bernien, B. Hensen, W. Pfaff, G. Koolstra, M.S. Blok, L. Robledo, et al., Heralded entanglement between solid-state qubits separated by three metres., Nature. 497 (2013) 86–90.

[12] T. Staudacher, F. Shi, S. Pezzagna, J. Meijer, J. Du, C. a Meriles, et al., Nuclear magnetic resonance spectroscopy on a (5-nanometer)^3 sample volume., Science. 339 (2013) 561–3.

[13] M. Geiselmann, M.L. Juan, J. Renger, J.M. Say, L.J. Brown, F.J.G. de Abajo, et al., Three-dimensional optical manipulation of a single electron spin., Nat. Nanotechnol. 8 (2013) 175–9.

[14] L.P. McGuinness, Y. Yan, a Stacey, D. a Simpson, L.T. Hall, D. Maclaurin, et al., Quantum measurement and orientation tracking of fluorescent nanodiamonds inside living cells., Nat. Nanotechnol. 6 (2011) 358–63.

[15] R. Igarashi, Y. Yoshinari, H. Yokota, T. Sugi, F. Sugihara, K. Ikeda, et al., Real-time background-free selective imaging of fluorescent nanodiamonds in vivo., Nano Lett. 12 (2012) 5726–32.

[16] G. Balasubramanian, I.Y. Chan, R. Kolesov, M. Al-Hmoud, J. Tisler, C. Shin, et al., Nanoscale imaging magnetometry with diamond spins under ambient conditions., Nature. 455 (2008) 648–51.

[17] J.R. Maze, P.L. Stanwix, J.S. Hodges, S. Hong, J.M. Taylor, P. Cappellaro, et al., Nanoscale magnetic sensing with an individual electronic spin in diamond., Nature. 455 (2008) 644–7.

[18] F. Dolde, H. Fedder, M.W. Doherty, T. Nöbauer, F. Rempp, G. Balasubramanian, et al., Electric-field sensing using single diamond spins, Nat. Phys. 7 (2011) 459–463.

[19] D.M. Toyli, C.F. de las Casas, D.J. Christle, V. V Dobrovitski, D.D. Awschalom, Fluorescence thermometry enhanced by the quantum coherence of single spins in diamond., Proc. Natl. Acad. Sci. U. S. A. 110 (2013) 8417–21.

[20] Y. Doi, T. Makino, H. Kato, D. Takeuchi, M. Ogura, H. Okushi, et al., Deterministic Electrical Charge-State Initialization of Single Nitrogen-Vacancy Center in Diamond, Phys. Rev. X. 4 (2014) 011057.

[21] K.-M.C. Fu, C. Santori, P.E. Barclay, R.G. Beausoleil, Conversion of neutral nitrogen-vacancy centers to negatively charged nitrogen-vacancy centers through selective oxidation, Appl. Phys. Lett. 96 (2010) 121907.

[22] B. Grotz, M. V Hauf, M. Dankerl, B. Naydenov, S. Pezzagna, J. Meijer, et al., Charge state manipulation of qubits in diamond., Nat. Commun. 3 (2012) 729.

[23] P. Siyushev, H. Pinto, M. Vörös, a. Gali, F. Jelezko, J. Wrachtrup, Optically Controlled Switching of the Charge State of a Single Nitrogen-Vacancy Center in Diamond at Cryogenic Temperatures, Phys. Rev. Lett. 110 (2013) 167402.

[24] C. Bradac, T. Gaebel, N. Naidoo, J.R. Rabeau, A.S. Barnard, Prediction and measurement of the size-dependent stability of fluorescence in diamond over the entire nanoscale., Nano Lett. 9 (2009) 3555–64.

[25] J.-M. Cui, X.-D. Chen, L.-L. Fan, Z.-J. Gong, C.-W. Zou, F.-W. Sun, et al., Generation of Nitrogen-Vacancy Centers in Diamond with Ion Implantation, Chinese Phys. Lett. 29 (2012) 036103.

[26] B.R. Smith, D.W. Inglis, B. Sandnes, J.R. Rabeau, A. V Zvyagin, D. Gruber, et al., Five-nanometer diamond with luminescent nitrogen-vacancy defect centers., Small. 5 (2009) 1649–53.

[27] S. Osswald, G. Yushin, V. Mochalin, S.O. Kucheyev, Y. Gogotsi, Control of sp2/sp3 carbon ratio and surface chemistry of nanodiamond powders by selective oxidation in air., J. Am. Chem. Soc. 128 (2006) 11635–42.

[28] J. Cebik, J.K. McDonough, F. Peerally, R. Medrano, I. Neitzel, Y. Gogotsi, et al., Raman spectroscopy study of the nanodiamond-to-carbon onion transformation., Nanotechnology. 24 (2013) 205703.

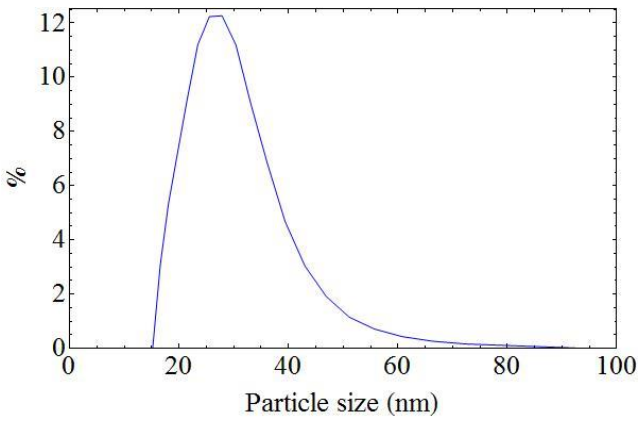

Figure 1. Particle-size distribution of nanodiamonds as measured by dynamic light scattering (DLS).

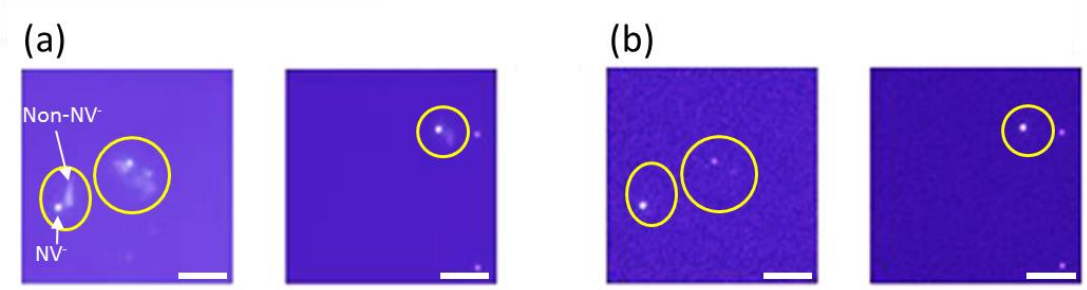

Figure 2. (a) Conventional fluorescence and (b) selective images of NV^-s at the same area in the sample [He^+, 60 keV, 1×10^{13}]. Yellow circles indicate an area of co-existence of fluorescence signals from NV^-s and non-NV^-s. The selective imaging as shown in (b) clearly eliminates extrinsic fluorescence. Scale bar shows 10 μm.

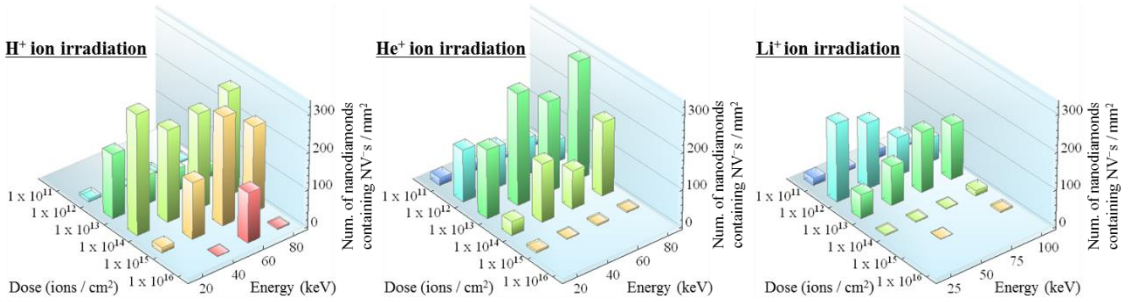

Figure 3. Numbers of nanodiamonds containing NV^-s created by ion irradiation of H^+, He^+ and Li^+ ions as a function of irradiation energy and dose. The bar height indicates the number per 1 mm^2. The Dose axis is a log scale.

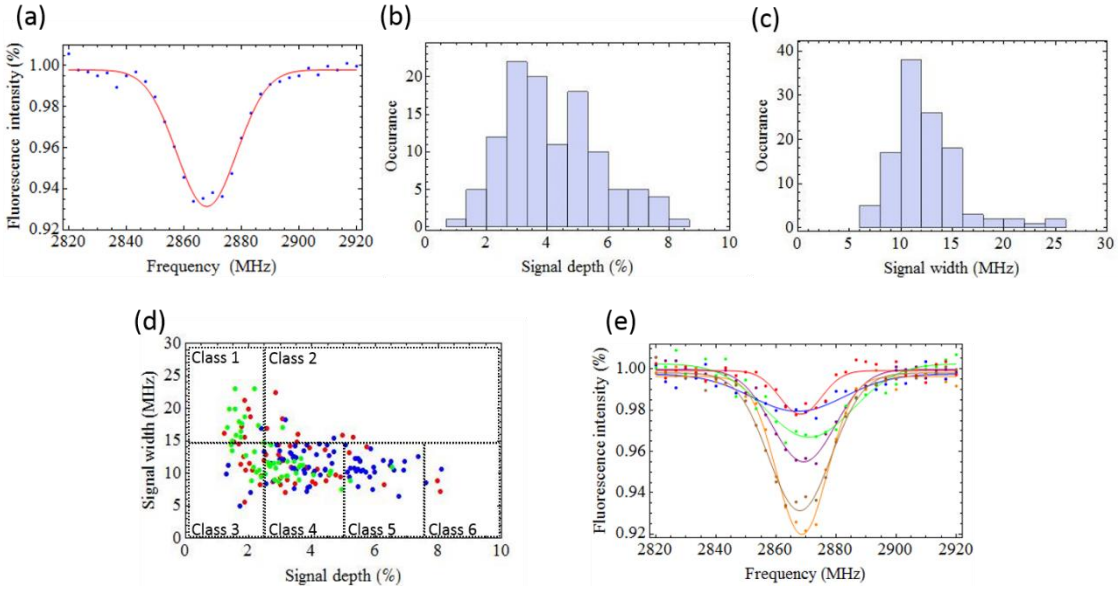

Figure 4. (a) Example of an ODMR spectrum fitted to a Gaussian function expressed by Eq.(1) in the main text. The fluorescence intensity is given as a ratio of the intensity at NV^-s taken with microwave irradiation divided by that without it. (b) and (c) Histograms of signal depth α and width $\Delta\nu$. (d) Correlation chart between α and $\Delta\nu$. The chart was divided into 6 categories. The results of He^+ ion irradiation at 80 keV, 1×10^{12} (red), 1×10^{13} (blue) and 1×10^{14} (green) are shown in this figure. (e) Examples of ODMR spectra picked from class 1 (blue), class 2 (green), class 3 (red), class 4 (purple), class 5 (brown) and class 6 (orange), together with their fits to Eq.(1).

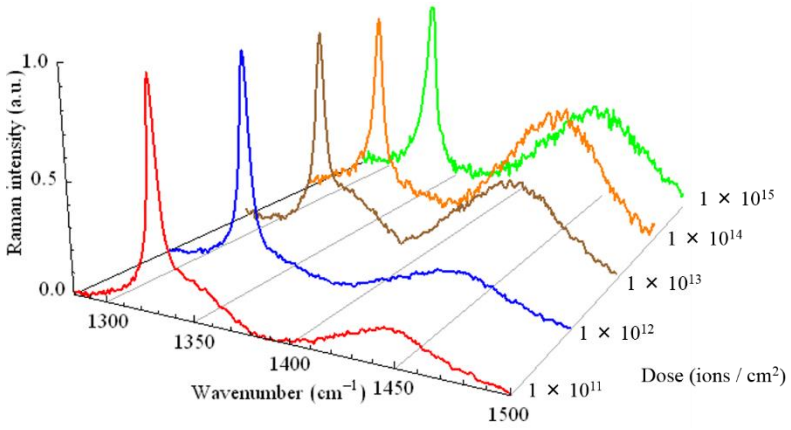

Figure 5. Examples of Raman spectra of nanodiamonds irradiated with He^+ ions at 20 keV and doses of 1×10^{11} (red), 1×10^{12} (blue), 1×10^{13} (brown), 1×10^{14} (orange) and 1×10^{15} (green) ions per cm^2. The signal intensities are normalized for comparison at 1332 cm^{-1}.

Table 1. Mean penetration depths and the distribution widths of stopped ions implanted into a diamond crystal of sufficient thickness. The calculation was made by SRIM. (a) H^+, (b) He^+, (c) Li^+ and (d) N^+ ion irradiations.

(a)

Energy keV	Range Å	Straggle Å	Vacancy / ion
20	1281	229	4.7
40	2135	248	5.4
60	2903	258	5.7
80	3647	298	6.2

(b)

Energy keV	Range Å	Straggle Å	Vacancy / ion
20	936	220	37
40	1594	287	44
60	2157	321	49
80	2671	357	51

(c)

Energy keV	Range Å	Straggle Å	Vacancy / ion
25	879	222	59
50	1607	320	76
75	2225	359	85
100	2773	406	91

(d)

Energy keV	Range Å	Straggle Å	Vacancy / ion
100	1150	218	190
150	1650	271	224
200	2126	293	245
250	2565	335	265

Table 2. Numbers of nanodiamonds containing NV^-s per 1 mm^2 versus irradiation energy and dose of (a) H^+, (b) He^+ and (c) Li^+ ions.

(a)

Energy keV	1×10^{11} Ions cm^{-2}	1×10^{12} Ions cm^{-2}	1×10^{13} Ions cm^{-2}	1×10^{14} Ions cm^{-2}	1×10^{15} Ions cm^{-2}	1×10^{16} Ions cm^{-2}
20	-	9	173	322	14	0
40	-	4	77	246	152	2
60	-	7	60	255	290	134
80	-	5	31	281	231	4

(b)

Energy keV	1×10^{11} Ions cm^{-2}	1×10^{12} Ions cm^{-2}	1×10^{13} Ions cm^{-2}	1×10^{14} Ions cm^{-2}	1×10^{15} Ions cm^{-2}	1×10^{16} Ions cm^{-2}
20	20	140	184	37	6	-
40	20	110	300	157	3	-
60	8	99	244	103	5	-
80	9	59	318	198	4	-

(c)

Energy keV	1×10^{11} Ions cm^{-2}	1×10^{12} Ions cm^{-2}	1×10^{13} Ions cm^{-2}	1×10^{14} Ions cm^{-2}	1×10^{15} Ions cm^{-2}	1×10^{16} Ions cm^{-2}
25	19	211	64	4	0	-
50	11	178	105	4	1	-
75	24	104	163	3	0	-
100	6	65	148	14	5	-

Table 3. Ratios of the number of nanodiamonds containing NV^-s classified in class 5 or 6 to the total numbers of nanodiamonds containing NV^-s. (a) H^+, (b) He^+ and (c) Li^+ ions.

(a)

Energy keV	1×10^{13} Ions cm^{-2}	1×10^{14} Ions cm^{-2}	1×10^{15} Ions cm^{-2}
20	0.06	0.11	-
40	0.1	0.30	0.00
60	0.13	0.28	0.15
80	0.00	0.32	0.00

(b)

Energy keV	1×10^{12} Ions cm^{-2}	1×10^{13} Ions cm^{-2}	1×10^{14} Ions cm^{-2}
20	0.05	0.18	-
40	0.12	0.29	0.00
60	0.15	0.44	0.05
80	0.11	0.40	0.04

(c)

Energy keV	1×10^{12} Ions cm^{-2}	1×10^{13} Ions cm^{-2}
25	0.01	0.00
50	0.03	0.00
75	0.01	0.00
100	0.00	0.01

Table 4. Crystal quality of nanodiamonds irradiated by (a) H^+ or (b) He^+ ion. The number in each column is a ratio of Raman signal intensity of sp^3 bonding carbon (1332 cm^{-1}) divided by that of disorder induced band peak (~1500 cm^{-1})(see Fig. 5).

(a)

Energy keV	1×10^{13} Ions cm^{-2}	1×10^{14} Ions cm^{-2}	1×10^{15} Ions cm^{-2}
20	1.34	0.75	-
40	2.95	1.58	1.04
60	3.49	1.11	0.44
80	2.38	2.36	1.30

(b)

Energy keV	1×10^{12} Ions cm^{-2}	1×10^{13} Ions cm^{-2}	1×10^{14} Ions cm^{-2}
20	2.61	1.06	-
40	4.46	1.22	0.61
60	3.78	1.65	0.88
80	5.89	1.24	0.70

Supplementary Material:

Effective Production of Fluorescent Nanodiamonds Containing Negatively-Charged Nitrogen-Vacancy Centers by Ion Irradiation

Shingo Sotoma,[†] Yohsuke Yoshinari,[‡] Ryuji Igarashi,[†] Akiyoshi Yamazaki,[§] Shige H. Yoshimura,[Δ] Hidehito Tochio,[†] Masahiro Shirakawa[†,‡] and Yoshie Harada*[,‡]

[†]Department of Molecular Engineering, Graduate School of Engineering, Kyoto University, Nishikyo-Ku, Kyoto 615-8510, Japan

[‡]Institute for Integrated Cell-Material Sciences (WPI-iCeMS), Kyoto University, Yoshida-Honmachi, Sakyo-ku, Kyoto 606-8501, Japan

[§]Takasaki Advanced Radiation Research Institute, Japan Atomic Energy Agency, 1233 Watanuki-machi, Takasaki, Gunma 370-1292, Japan

[Δ]Graduate School of Biostudies, Kyoto University, Yoshida-konoe-cho, Sakyo-ku, Kyoto 606-8501, Japan

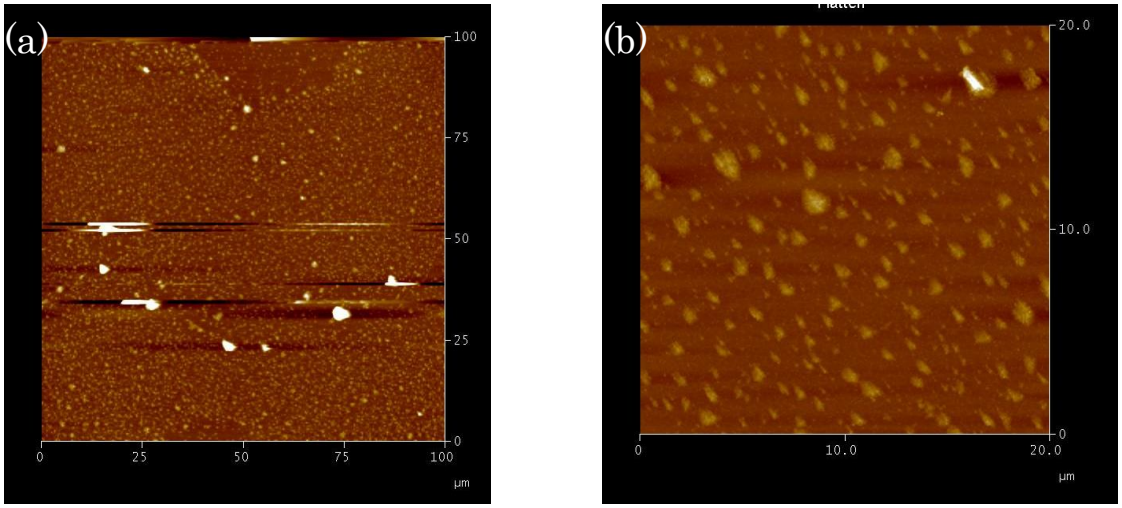

Figure S1. (a)AFM image of spin-coated nanodiamonds on silicon wafer. (b) Close-up image of (a).